Rare Metal Materials and Engineering

Available online at **www.rmme.ac.cn**

Science Press

Cite this article as: Rare Metal Materials and Engineering

ARTICLE

DOI: 10.12442/j.issn.1002-185X.20240460.

The Influence of Current Density and Copper Ion Concentration on the Properties of Electrodeposited Cu-Ni Coatings

Xuyan Guo [1, =], Zhuangzhuang Xiong [1, =], Guixiang Wang [1, 3, z], Qiang Zhou [1], Yanxiong Wu [1], Delong Kong [2, z], Fuqiu Ma [1], Ruizhi Wu [3]

[1] Yantai Research Institute, Harbin Engineering University, Yantai 264006, China; [2] Chemical Engineering and Materials Science, Zaozhuang University, Zaozhuang 277160, China; [3] Key Laboratory of Superlight Materials and Surface Technology, Harbin Engineering University, Harbin 150001, China

Abstract: This article investigates a straightforward, highly effective, and eco-friendly technique for preserving carbon steel surfaces against corrosion, by depositing Cu-Ni alloy coatings on the workpiece's surface to impede corrosive medium. The effects of current density and Cu^{2+} concentration on the composition, morphology, and composition of the coating were investigated using scanning electron microscopy, X-ray energy dispersive spectroscopy, Vickers hardness tester, friction and wear tester, and electrochemical testing. A cauliflower like Ni rich protrusion structure appears on the coating surface. The lower current density and Cu^{2+} concentration affect the Vickers hardness and wear resistance of the coating by affecting the grain microstructure and Cu/Ni content, both leading a decrease in hardness and wear resistance. When the current density is 10 mA/cm^2 and the Cu^{2+} concentration is 0.1 mol/L, the corrosion current density of the deposited sample reached 1.389×10^{-5} A·cm^{-2}, and its surface corrosion damage was significantly less than that of the sample without coating after 24 h of salt spray test. Research on the deposition mechanism indicates that Cu^{2+} undergoes instantaneous nucleation under diffusion control, tending towards vertical growth and forming cauliflower-like protrusions, while Ni^{2+} is controlled by electrochemistry to discharge uniformly across the surface.

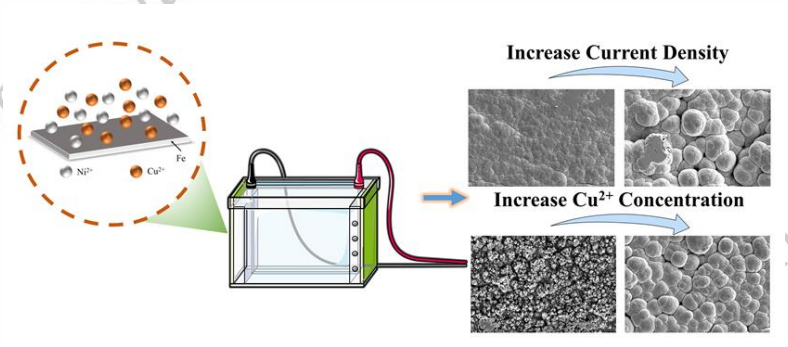

Key words: Cu-Ni coatings, Corrosion protection, Morphology, Performance

In the marine environment, carbon steel structural elements are subject to significant corrosion challenges. Copper-Nickel

Received date:
Foundation item: the Key R&D Program of Shandong Province, China (2023SFGC0101), NSFC(51971071, 52075112 and 52261135538), Fundamental Research Projects of Science & Technology Innovation and development Plan in Yantai City (No.2022JCYJ023).
Corresponding author: Guixiang Wang, Ph.D., Professor, Yantai Research Institute, Harbin Engineering University, Yantai 264006, China, E-mail: wangguixiang@hrbeu.edu.cn

(Cu-Ni) alloys, renowned for their commendable mechanical properties[1-3], antibacterial attributes[4, 5], and corrosion resistance[6-10], find extensive application in marine machinery, pipelines, and vessels. Research results have demonstrated that Cu-Ni alloys, with varying elemental compositions, exhibit noteworthy corrosion resistance in seawater environments[11, 12]. Currently, established methods for fabricating Cu-Ni film layers on metal encompass thermal spraying[13], electrodeposition[14], laser cladding[15], and so on. Electrodeposition has gained widespread adoption for its economic efficiency and straightforward operation. Consequently, the electrodeposition of a Cu-Ni film on carbon steel structural elements emerges as a viable solution to address the issue of seawater corrosion in workpieces.

Extensive research on the electrodeposition process of Cu-Ni alloys boasts a longstanding history. The alloy coating produced via electrodeposition is intricately influenced by various process parameters, including electrolytic cell specifications, metal ion concentration ratios, complexing agents, electrode potential, and deposition current. Chlorides and sulfates stand out as two prevalent plating solution systems. To circumvent the emission of chlorine gas induced by oxidation of chloride ions in the solution as well as the equipment corrosion[16], this study opts for the widely employed Watt-type (sulfate) plating solution. However, employing copper and nickel sulfate alone fails to achieve the codeposition of the two ions due to the substantial standard reduction potential difference (Cu = +0.34 V vs. SHE, Ni = −0.23 V vs. SHE) between them. Consequently, the addition of a complexing agent to the plating solution is imperative to realize codeposition[17]. Various complexing agents, including lactic acid[18], citrate, and pyrophosphate[19], have been utilized for the electrodeposition of Cu-Ni alloys. Among these, citrate, derived from biological sources, boasts notable advantages in terms of environmental friendliness, low toxicity, and high economic efficiency[20]. Another favorable aspect of citrate is its multifunctionality, serving not only as a complexing agent but also as a pH regulator, buffer, brightener, etc.[21]. Therefore, compared to alternative complexing systems, there is no necessity to introduce additional additives. Chassaing's investigation into citric acid complexation systems under alkaline condition[22] revealed that the discharge of Cu was governed by diffusion. The model proposed by the author effectively replicated the test results of the polarization curve. Subsequent work by Rode[23] not only corroborated Chassaing's theory but also suggested novel adsorbents based on it, highlighting that lower Cu^{2+} concentrations contribute to sustaining the stability of the plating solution. Consequently, when formulating the plating solution, it is imperative to ensure a high Ni^{2+}/Cu^{2+} ratio. Nevertheless, the research lacks actual coating data, and there is a deficiency in the analysis that integrates micro morphology and composition, which imposes certain limitations.

Many scholars have studied the theory of ion electrocrystallization to elucidate the formation mode of tissue morphology. Milchev's research on the Cu^{2+} deposition process has delineated an I-t relationship under two mechanisms: ion transfer and charge transfer[24, 25]. Isaev has furnished precise solutions for both instantaneous and continuous nucleation problems, encompassing the processes of crystal nucleus formation and growth, whose parameters can be extracted from the initial segment of the I-t curve[26].

The purpose of this work is to develop a green and efficient surface anti-corrosion technology for carbon steel. We selected an environmentally-friendly acidic citric acid plating solution to deposit a layer of Cu-Ni alloy coatings on carbon steel workpieces, and examined the influence of current density and Cu^{2+} concentration on the composition, morphology, and performance of the coating. Additionally, the study delves into elucidating the formation mode of the deposition microstructure morphology by scrutinizing the deposition mechanism of Cu^{2+} and Ni^{2+}. The findings of this investigation hold significant reference value for developing a sophisticated Cu-Ni alloy electroplating technique and enhancing the application of Cu-Ni alloy protective coatings in marine anticorrosion.

1 Experiment

1.1 Electroplating experiment

Four distinct Cu^{2+} concentrations and four varied current densities were employed to fabricate Cu-Ni alloy samples on cold-rolled steel plates. Other experimental conditions remained constant except for Cu^{2+} concentration and current density. The specific data are detailed in Table 1. pH values were adjusted to the desired levels using sulfuric acid and sodium hydroxide.

Table. 1 Composition of Cu-Ni alloy plating solution and experimental conditions

Composition	Concentration and condition
$NiSO_4 \cdot 6H_2O$	157.7 g/L
Sodium Citrate	88.2 g/L
Sodium Dodecyl Sulfate	1 g/L
Temperature	50 ℃
Time	10 min
Stirring Speed	200 r/min
pH	5.0

Conduct electrodeposition experiments on all experimental groups using a constant current power supply. The Cu^{2+} concentration and current density parameters for different groups are detailed in Table 2. Each experimental group should undergo deposition at least three times to ensure adequate reproducibility of the results. A soluble anode is constituted by copper and nickel plates, while the cathode consists of a carbon steel specimen.

Table. 2 Cu^{2+} Concentration and Current Density of Different Experimental Groups.

No.	$c(Cu^{2+})$ /(mol/L)	j/ (mA/cm^2)	No.	$c(Cu^{2+})$ /(mol/L)	j/ (mA/cm^2)
A	0.12	10	E	0.01	20
B	0.12	15	F	0.05	20
C	0.12	20	G	0.1	20
D	0.12	30	H	0.15	20

Prior to each experiment, employ an ethanol solution for ultrasonic cleaning of the test piece to eliminate surface grease from the carbon steel. Subsequently, utilize a 5 wt.% nitric acid solution for acid washing to eliminate the oxide layer on the test piece's surface and activate the substrate. Between each aforementioned step, thoroughly wash the test piece's surface with deionized water to prevent the carryover of residual reagents from the preceding step to the subsequent one.

1.2 Composition, morphology and performance testing of coatings

Scanning electron microscopy (SEM) was employed to examine the microstructure of the coating, and Energy Dispersive Spectrometer (EDS) analysis was conducted on the coating surface to delineate the elemental composition of the coating surface.

A digital microhardness tester was utilized to assess the Vickers hardness of the prepared coating. The hardness value of the sample was calculated by determining diagonal length of the indentation on a 500g weight. Average value of three tests on the same sample was adopted in this paper.

A pin disc friction and wear testing machine was employed to assess the tribological performance of the coating under a load weight of 300 g. 10 min friction test was conducted and the friction coefficient of the coating surface was then calculated.

Throughout the neutral salt spray (NSS) test, the temperature was kept at 35±2℃ and a 5 wt.% NaCl solution was used as the test solution. After 24 hours of testing, the test piece was retrieved from the box for SEM testing.

The contact angle (CA) test employs a video optical contact angle measuring instrument. It involves placing 10 μL droplets on the surface of the prepared coating, capturing photos, and subsequently calculating the contact angle of the droplets on the coating surface through computer analysis.

1.3 Electrochemical test

All electrochemical experiments were carried out using the CHI760E electrochemical workstation with a conventional three-electrode system. Both electrochemical impedance spectroscopy (EIS) and polarization curve tests were performed on carbon steel and Cu-Ni alloy coatings. In this setup, the specimen served as the working electrode, a saturated calomel electrode (SCE) acted as the reference electrode, and a platinum wire was employed as the counter electrode. These experiments were conducted using a 3.5 wt.% NaCl aqueous solution at room temperature (20℃). EIS and polarization curve tests were initiated when the fluctuation value of the open circuit potential (OCP) was less than 5 mV within 5 min. For EIS, the testing potential was set at the open circuit potential, with a testing frequency ranging from 10^{-2} to 10^5 Hz and an amplitude of 5 mV. Data fitting was performed using the ZSimpWin software. The scanning speed for polarization curve testing was set at 5 mV·s^{-1}, and the voltage testing range was defined as ±0.3 V around the open circuit potential. The corrosion current density and corrosion potential were calculated using Tafel extrapolation method.

To investigate the nucleation and growth of Ni^{2+} and Cu^{2+} on a glassy carbon electrode (GCE), chronoamperometry was employed. GCE and SCE were employed as the working electrode and reference electrode, respectively. Copper and nickel plates served as the counter electrodes for the experimental in terms of Ni^{2+} and Cu^{2+}, respectively. The electrode surface area of GCE was 0.0707 cm^2. In the chronoamperometric method, the potential was stepped from the OCP to the applied potential. Before each experiment, GCE was polished on a polishing cloth with added nano alumina particles to ensure good repeatability of the experiment.

2 Results and Discussion

2.1 Microscopic morphology and composition of coating

Figure 1 shows the morphology of Cu-Ni alloy coatings magnified by 5000 times at various current densities and Cu^{2+} concentrations. It is evident that within the current density range of 10-30 mA/cm^2, the sediment manifests as fine and densely packed cauliflower-like structures. With the escalation of current density, the morphology of these cauliflower-like protrusions becomes more pronounced. Higher deposition current density, as depicted in the figure, results in gaps between the cauliflower structures, rendering them less compact compared to samples with lower deposition current density. Overall, the variation in current density influences the interstitial space of the structure, and with increasing current density, the cauliflower-like structure transitions from being dense to more loosely arranged.

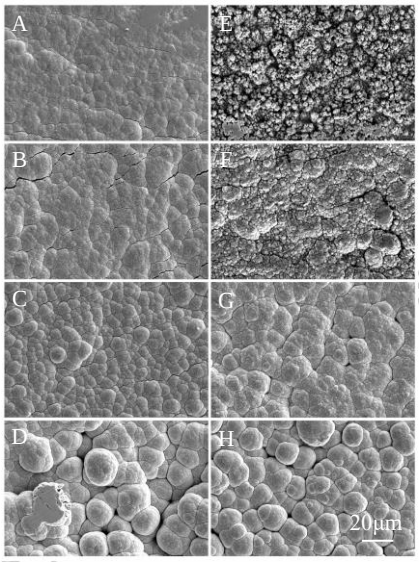

Fig. 1. Micromorphology of Cu-Ni coating under different current densities and Cu^{2+} concentrations.
A: 10 mA/cm^2, B: 15 mA/cm^2, C: 20 mA/cm^2, D: 30 mA/cm^2, E: 0.01 mol/L, F: 0.05 mol/L, G: 0.1 mol/L, H: 0.15 mol/L

Similarly, we examined the microstructure of the coating at varying Cu^{2+} concentrations. At very low Cu^{2+} concentrations (E), the cauliflower structure was replaced by sharp protrusions. However, with a further increase in Cu^{2+} concentration, the cauliflower-like structure reappeared, and the structure became larger and looser with a continued increase of copper ion in the solution. At a specific Cu^{2+} concentration in the plating solution (F), increasing the Cu^{2+} concentration exhibited a similar effect to increasing the current density.

From this, it can be inferred that the condition for the appearance of the cauliflower structure in the coating is the presence of sufficient copper in the plating solution. When this condition is met, augmenting the copper content will contribute to the expansion and bulging of the cauliflower structure. This suggests that the formation of cauliflower-like protrusions and depressions is related to the distribution of copper and nickel elements in the coating. This connection leads to the emergence of the cauliflower-like structure in the coating when the concentration of Cu^{2+} is increased, facilitating the process of growth and protrusion. This phenomenon has been addressed in prior studies, and experiments by Goranova[27] have indicated that the Cu-Ni alloy coating obtained through deposition forms a solid solution of Cu and Ni elements, albeit with a certain element enrichment in different structures.

To confirm the enrichment of this element in the coating obtained by acidic citric acid system deposition, EDS point scanning was performed on two groups of samples with Cu^{2+} concentrations of 0.01 mol/L and 0.15 mol/L. The scanning test results are shown in Figure 2. Since the main elements in the coating are only copper and nickel, Ni wt.% can be considered as 100-Cu wt.%. The results indicate that in an acidic citric acid system, Cu will accumulate on the raised surface and Ni will accumulate in the depression, which is not affected by the formation of cauliflower structure. Moreover, before the formation of cauliflower like structures, sharp protrusions had stronger Cu enrichment ability, and the difference in Cu wt.% between the protrusions and depressions in the No. E experimental group reached 70.92 wt.%. This indicates that within a wide range of Cu^{2+} concentration, the formation of micro morphology protrusions in the coating structure is controlled by copper deposition.

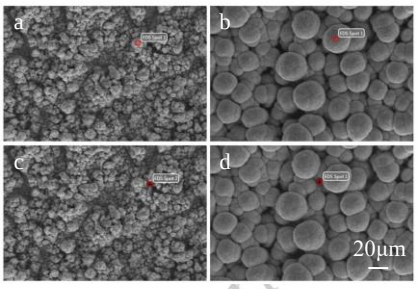

Fig. 2. Scanning electron microscopy images of two groups of samples, No. E (a, c) and No. H (b, d):
a Cu 92.98 wt.%; b Cu 95.23 wt.%; c Cu 22.06 wt.%; d Cu 42.91 wt.%

To investigate the elemental composition of Cu-Ni alloy coatings under different current densities and Cu^{2+} concentrations, EDS mapping tests were conducted on all samples, and the results are depicted in Table 3. As the current density changed from 10 mA/cm^2 to 30 mA/cm^2, the Ni wt.% in the coating gradually increased, corresponding to the progressive protrusion and dispersion of the cauliflower structure in the scanning electron microscope image of the coating. After the Cu^{2+} concentration increased from 0.01 mol/L to 0.05 mol/L, a cauliflower-like structure emerged in the coating. Continuing to increase the Cu^{2+} concentration resulted in a decrease in Ni wt.% in the coating structure, but the degree of dispersion of the cauliflower-like structure did not decrease with a reduction in Ni wt.%. This indicates that it cannot be simply assumed that an increase in Cu wt.% or Ni wt.% in the plating structure leads to a change in the cauliflower-like structure, and the current density and Cu^{2+} concentration have different effects on the cauliflower-like structure.

Based on the EDS results, it is evident that the protrusions of the cauliflower-like structure are primarily composed of Cu, indicating that the deposition behavior of Cu is the main factor controlling the cauliflower-like structure of the coating. As the concentration of Cu^{2+} in the plating solution increases, the Cu wt.% of the coating increases, leading to the gradual formation and protrusion of cauliflower-like structures. In the No. A ~ D experimental group, the plating solution contains a sufficient Cu^{2+} concentration to ensure the formation of cauliflower-like structures. In this scenario, increasing the current density results in a decrease in Cu wt.% in the plating layer. Since the cauliflower-like structure is primarily controlled by Cu depo-

sition, the decrease in Cu wt.% leads to a reduction in the number of cauliflower-like structures formed, while high current density further increases the size of cauliflower-like structures. These factors contribute to the protrusion and dispersion of cauliflower-like structures in the coating. The morphology of group No. D in Figure 1 confirms this hypothesis, showing that under high current density, the number of cauliflower-like structures in the coating structure decreases, and the size increases.

Table 3 Surface Cu wt.% and Ni wt.% of samples from different experimental groups.

No.	Cu (wt.%)	Ni (wt.%)	No.	Cu (wt.%)	Ni (wt.%)
A	97.28	2.72	E	14.73	85.27
B	89.94	10.06	F	48.15	51.85
C	66.93	33.07	G	73.70	26.30
D	61.14	38.86	H	91.12	8.88

2.2 Corrosion resistance of coating

Electrochemical tests were conducted on coatings deposited at different current densities and Cu^{2+} concentrations, and Figure 3 illustrates the EIS and polarization curves. The electrochemical corrosion parameters of the coating, acquired from dynamic potential polarization measurements, are presented in Table 4.

The fitting circuit chosen for impedance fitting is represented as R(Q(R(QR))), and the circuit diagram is depicted in Figure 3e. Here, R_s represents the solution resistance, CPE_c denotes the capacitance of the Cu-Ni coating, R_c signifies the resistance of the Cu-Ni coating, R_{ct} is the charge transfer resistance, and CPE_{dl} represents the double-layer capacitance at the interface between the Cu-Ni coating and the iron substrate.

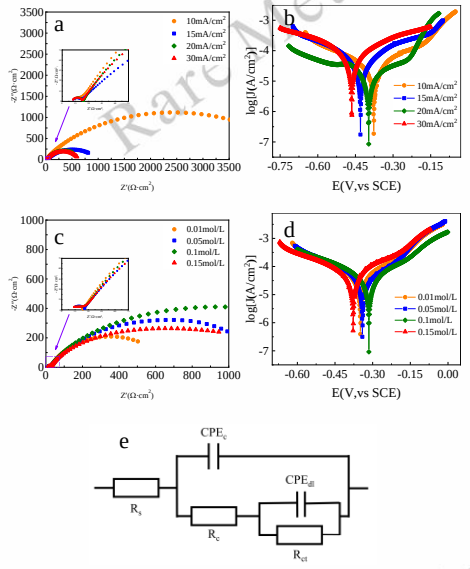

Fig. 3. EIS and polarization curves of coatings under different current densities and Cu^{2+} concentrations.

Under different current densities: a Nyquist curve, b polarization curve; under different Cu^{2+} concentrations: c Nyquist curve, d polarization curve.

Table 4: Electrochemical parameters calculated from the curves b and d in Figure 3.

No.	E_{corr}(V)	i_{corr}(A/cm^2)	No.	E_{corr}(V)	i_{corr}(A/cm^{-2})
A	−0.377	3.536×10^{-5}	E	−0.315	8.379×10^{-5}
B	−0.430	3.599×10^{-5}	F	−0.349	5.808×10^{-5}
C	−0.397	4.234×10^{-5}	G	−0.341	4.711×10^{-5}
D	−0.464	7.416×10^{-5}	H	−0.378	6.908×10^{-5}

All experimental groups exhibit Nyquist curves with one large and one small capacitive arc, aligning well with the fitting circuit represented by R(Q(R(QR))). The smaller arc radius corresponds to the film resistance Rc, representing the penetration of the corrosive medium through the entire Cu-Ni alloy coating. The larger arc radius signifies the size of the interface charge transfer resistance Rct. Notably, the charge transfer resistance at a current density of 10 mA/cm^2 is significantly higher than that of the experimental group with higher current density. This suggests that the coating deposited at a current density of 10 mA/cm^2 is more resistant to Cl^- penetration in a Cl^- corrosive environment, providing enhanced protection for the iron substrate. This observation is supported by the Bode mode diagram, where the low-frequency mode values of the experimental group with a current density of 10 mA/cm^2 show significant improvement compared to other groups, indicating overall higher corrosion resistance of the film layer. Electrochemical parameters calculated from the polarization curves further indicate that reducing the current density leads to a decrease in the corrosion current density of the coating. This implies that, when exposed to corrosive media, samples with low current density are less prone to corrosion damage and exhibit higher corrosion resistance. The higher Cu wt.% at low current density contributes to increasing corrosion resistance. Additionally, the microstructure of the coating plays a role, where higher current density results in larger cauliflower-like structures with increased gaps between them. In comparison to dense and compact structures under low current density, larger gaps facilitate the entry and exit of corrosive ions, making ion penetration easier and accelerating material corrosion. This is reflected in the electrochemical test results, where high current density samples exhibit lower charge transfer resistance and impedance mode values.

The EIS and polarization curves of coatings deposited with different Cu^{2+} concentrations reveal that the corrosion resistance of the coatings does not exhibit a monotonic change with Cu^{2+} concentration in the plating solution but rather reaches a peak value. Calculating the corrosion current density from the polarization curve indicates that the coating exhibits the highest corrosion resistance at a Cu^{2+} concentration of 0.1 mol/L. This phenomenon can be explained by considering the microstructure. When the Cu^{2+} concentration is below 0.05 mol/L, the coating comprises sharp protrusion-like structures. Due to the low Cu content in the plating solution, the deposition of cop-

per-rich protrusions is relatively limited, resulting in a sparse coating structure that offers inadequate protection against corrosive media and low corrosion resistance. As the Cu^{2+} concentration surpasses 0.05 mol/L, a cauliflower-like structure begins to emerge in the coating. With further increases in Cu^{2+} concentration, the cauliflower structure gradually replaces all sharp protrusions, resulting in a coating composed of a dense cauliflower-like structure and achieving the highest corrosion resistance. As the Cu^{2+} concentration continues to increase, gaps develop between cauliflower-like structures, leading to a transition from dense to sparse coating structures. This transition adversely affects corrosion resistance, outweighing the increase in Cu wt.% in the coating, resulting in a reduction in capacitance arc radius and an increase in corrosion current density in the polarization curve. Additionally, it is observed that when the Cu^{2+} concentration exceeds 0.1 mol/L, variations in sample impedance and polarization curve test results due to changes in Cu^{2+} concentration become relatively small. This suggests that the impact of the transformation from sharp protrusions to cauliflower structure on corrosion resistance is more significant than that of the cauliflower structure itself.

The parameters representing the experimental group with the optimal corrosion resistance in the previous tests were chosen for the electrodeposition experiment, maintaining a current density of 10 mA/cm^2 and a Cu^{2+} concentration of 0.1mol/L. Comparative results with the undeposited carbon steel matrix are depicted in Figure 4a, b, c, and d, illustrating the macroscopic and 2000 times microscopic morphologies of the sample after 24 hours of salt spray exposure. Figure 4e displays the polarization curve, while Table 5 presents the electrochemical corrosion parameters of the prepared Cu-Ni coating calculated through potentiodynamic polarization measurement. The corrosion potential of the prepared Cu-Ni coating shifts forward by approximately 0.2 V, and the corrosion current density decreases by an order of magnitude. Salt spray experiments confirm that, under the same NaCl concentration, Cu-Ni coatings exhibit superior resistance to corrosion damage. This substantiates that electrodepositing Cu-Ni coatings on carbon steel structural components effectively mitigates losses due to corrosion in seawater environments and, to some extent, expands the application of carbon steel structural components in the marine field.

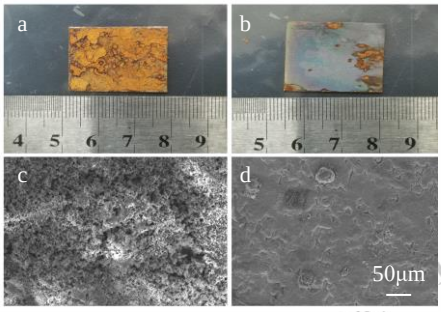

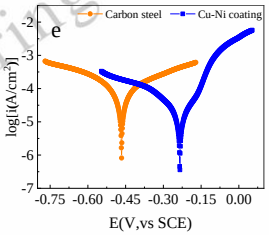

Fig. 4. Comparison of polarization curves and 24 h salt spray experimental results between Cu-Ni coating (b, d) and carbon steel substrate (a, c).

a. b: Macro appearance, c, d: Microscopic morphology, e: polarization curve.

Table 5: Electrochemical parameters calculated from the curve e in Figure 4.

Sample	E_{corr}(V)	I_{corr}(A·cm^{-2})
Carbon steel	−0.466	1.001×10^{-4}
Cu-Ni coating	−0.234	1.389×10^{-5}

2.3 Mechanical properties and surface properties of coatings

Vickers hardness tests were conducted on samples deposited under various current densities and Cu^{2+} concentrations, and the results are illustrated in Figures 5a and c. Figures 5b and d depict the tribological test outcomes for samples deposited under different current densities and Cu^{2+} concentrations. Upon comparing Figure 5a and c, it is evident that the hardness of the coating is not significantly influenced by the current density. This could be attributed to the minor impact of altering the current density on the Ni wt.% of the coating. Another explanation is that the density of the cauliflower-like structure is not the primary factor affecting the Vickers hardness of the coating. Upon observing Figure 5c, it is noticeable that with the increase in the Cu/Ni ratio in the plating solution, the overall hardness of the coating exhibits a decreasing trend, influenced by the properties of copper and nickel. The Cu-Ni alloy formed through electrodeposition is a solid solution, and the two metals can form an infinite solid solution. Copper, being a wear-resistant material, possesses good flexibility but has a lower hardness compared to nickel. As the Cu wt.% in the coating gradually increases, the hardness inevitably decreases. However, we also observed that the Vickers hardness of the coating showed slight changes between 0.1 mol/L and 0.15 mol/L in Cu^{2+} concentration, even though a complete cauliflower-like structure had already formed during scanning electron microscopy testing at this point. This indicates that the sharp protrusion structure at low Cu^{2+} concentration contributes more to the hardness than the cauliflower-like structure. Once the coating structure completes the transformation from sharp protrusion to cauliflower-like structure, the overall hardness no longer changes significantly.

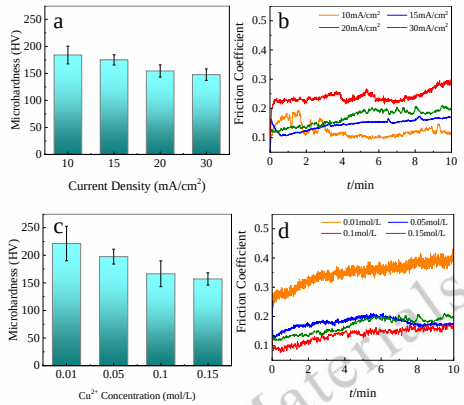

Fig. 5. Vickers hardness and friction coefficient curves of coatings under different current densities and Cu^{2+} concentrations.

The curve in Figure 5b indicates that, in general, increasing the deposition current density leads to an elevation in the friction coefficient of the coating. When combined with microstructure analysis, it becomes evident that the augmented gaps in cauliflower-like structures contribute to increased surface roughness of the coating. However, EDS mapping tests on the coating revealed that, in this scenario, the Cu wt.% of the coating gradually decreased. This implies that the impact of structural changes on the wear resistance of the coating outweighs the contribution of the wear-resistant metal Cu wt.% in the binary alloy coating.

In Figure 5d, the experimental group with a Cu^{2+} concentration of 0.01 mol/L exhibits a high friction coefficient at the beginning of the friction test, and the friction coefficient undergoes a sharp change as the experiment progresses. Microstructure analysis indicates that, compared to the cauliflower-like structure, the sharp protrusion structure is rougher, and the lower Cu wt.% in the coating also results in the absence of a wear-resistant copper-rich structure. These factors contribute to the overall friction coefficient of the coating being significantly higher than other experimental groups. However, the difference in friction coefficient between the other experimental groups after a period of wear is not significant, suggesting that similar to hardness, changes in cauliflower structure have little effect on wear resistance.

To further investigate the impact of the process on surface properties, water contact angle tests were conducted on samples deposited under different current densities and Cu^{2+} concentrations, and the results are depicted in Figure 6. It is observed that the water contact angle of the coating does not change significantly under different current densities but generally decreases with an increase in current density. The coating structure deposited under high current densities has larger microscopic dimensions, and the sparse structure leads to a rough coating, resulting in a slight decrease in its hydrophobicity.

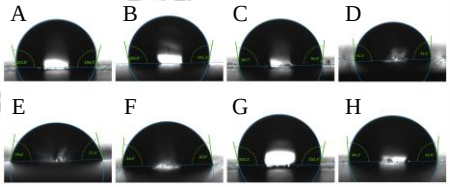

Fig. 6. Water CA of coatings under different current densities and Cu^{2+} concentrations.

When the concentration of copper ions is altered, the water contact angle changes more significantly, with a notable decrease at extremely low copper ion concentrations. This suggests that the sharp protrusion structure of the coating contributes much less to surface hydrophobicity than the cauliflower-like structure, and the substantial difference between the two structures results in a significant variance in hydrophobicity. Concurrently, the test results of the water contact angle align well with the earlier electrochemical test. The hydrophobicity of the coating to some extent affects its ability to block the infiltration of corrosive media, thereby impacting its corrosion resistance.

2.4 Electro crystallization mechanism

Choose a plating solution with a Cu^{2+} concentration of 0.1 mol/L and employ this solution as the electrolyte to investigate the electrocrystallization mechanism of Cu^{2+} and Ni^{2+}. The deposition type of Cu^{2+} and Ni^{2+} can be ascertained by examining the j-t relationship during the initial nucleation process[28]. When I_n-t follows a linear relationship, there are four types of nucleation depending on the value of n. When the growth of crystals is controlled by electron transfer, the nucleation type of the system is instantaneous nucleation when n is 1/2, and continuous nucleation when n is 1/3. When the growth of crystals is controlled by the transfer of reactant ions, the nucleation type of the system is instantaneous nucleation when n is 2, and continuous nucleation when n is 2/3.

The applied potential in both systems is slightly negative compared to the deposition potential and gradually increases from the OCP to the applied potential. Figure 7a illustrates the current density transient curves under different applied potentials of Cu^{2+}, while Figure 7b presents the logarithmic relationship curve of the transient early current time. The overall change in steady-state current is not significant, suggesting stable current values under different applied potentials. This indicates that the deposition of Cu^{2+} is controlled by diffusion steps. The curve with an applied potential of −0.9 V effectively demonstrates the initial nucleation behavior of Cu^{2+} deposition, revealing that copper deposition in this system follows diffusion-controlled instantaneous nucleation. Figure 7c depicts the current transient curves under different applied potentials of Ni^{2+}, and Figure 7d shows the logarithmic relationship curve of the transient early current time. The notable difference in steady-state current under various deposition potentials indicates that the deposition of Ni^{2+} is controlled by electrochemical steps. According to the curve with a deposition potential of −1.4

V, it can be determined that the deposition type of Ni^{2+} is instantaneous nucleation controlled by electrochemistry.

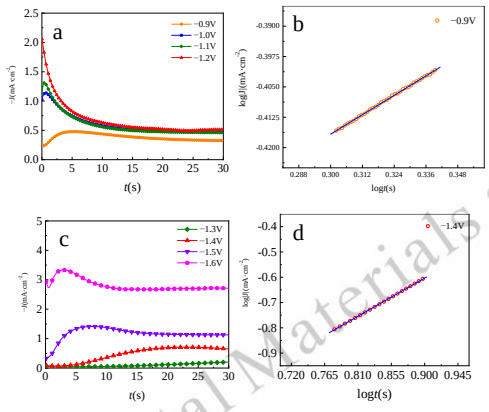

Fig. 7. Current time curve of Cu^{2+} and Ni^{2+} (a, c) and logj and logt curves in the early stage of current transient of Cu^{2+} and Ni^{2+} (b, d).

The coating's microstructure can now be elucidated based on the initial nucleation behavior of ions. The distinct deposition mechanisms of copper and nickel contribute to the unique morphology of Cu-Ni alloy coatings and also lead to variations in current density that impact the composition of the coatings.

The deposition of Cu is governed by diffusion, making the growth of copper more susceptible to variations in plating solution concentration. In regions where diffusion is more favorable, copper deposition is more likely to take place, manifesting in the actual coating as vertically grown crystals with higher copper content, ultimately giving rise to a cauliflower-like structure. The Cu wt.% in the alloy coating structure is more influenced by the deposition behavior of another metal. The deposition of Ni is governed by electrochemistry and remains unaffected by diffusion. Ni nucleates in areas with charge transfer, exhibiting a propensity for planar growth. It is evident that there is a higher concentration of nickel in the bottom layer and the depressions within the coating. Additionally, owing to the considerably higher nickel content in the plating solution compared to copper, nickel ions in the solution that are not complexed with citric acid lack preferential nucleation sites, resulting in random nucleation. Furthermore, this is reflected in the observation that changing the current density directly influences the deposition of Ni, with an increase in current density leading to a significant rise in the Ni wt.% in the coating.

3 Conclusions

This study demonstrates a green and efficient anti-corrosion technology for carbon steel in the marine field. Key findings are as follows:

(1) The Cu-Ni alloy coatings in the study exhibit a prevailing cauliflower-like structure, with structural characteristics influenced by varying current densities and Cu^{2+} concentrations. This coating effectively prevents the corrosion damage of Cl^- to the substrate, with a minimum corrosion current density of 1.389×10^{-5} A·cm^{-2}. After 24 h salt spray testing, the corrosion area of the coating is significantly reduced compared to the sample without coating coverage.

(2) Changing the current density and Cu^{2+} concentration can obtain Cu-Ni alloy coatings with different properties. Increasing the deposition current density, the corrosion current density of the coating changed from 3.536×10^{-5} A·cm^{-2} to 7.416×10^{-5} A·cm^{-2}, the hardness changed from 184.0 HV to 147.7 HV, and the water contact angle changed from 103.7° to 91.7°. Corrosion resistance and hydrophobicity exhibit an initial increase followed by a decline with higher Cu^{2+} concentration, while hardness and wear resistance generally decrease with increased Cu^{2+} concentration.

(3) The protrusions in the microstructure of the coating are rich Cu structure, while the depressions are rich Ni structure. The study of electrocrystallization mechanism shows that the deposition of Cu^{2+} is an instantaneous nucleation controlled by diffusion, while the deposition of Ni^{2+} is a instantaneous nucleation controlled by electrochemistry.

References

1 E. Pellicer, A. Varea, S. Pané, K. M. Sivaraman, B. J. Nelson, S. Suriñach, M. Baró, and J. Sort, Surf. Coat. Technol., 205 (23-24), 5285-5293 (2011).

2 X. Zhang, Y. Ma, N. Lin, X. Huang, R. Hang, A. Fan, and B. Tang, Surf. Coat. Technol., 232 515-520 (2013).

3 M. Alizadeh and H. Safaei, Appl. Surf. Sci., 456 195-203 (2018).

4 Y. Wang, X. Lu, N. Yuan, and J. Ding, J. Alloys Compd., 849 (2020).

5 F. Da Silva, N. Cinca, S. Dosta, I. Cano, J. M. Guilemany, C. Caires, A. Lima, C. Silva, S. Oliveira, and A. Caires, Surf. Coat. Technol., 361 292-301 (2019).

6 R. Song, S. Zhang, Y. He, T. He, H. Li, B. Liu, Z. Zhang, and Y. He, Colloids and Surfaces A: Physicochemical and Engineering Aspects, 649 (2022).

7 Z. Lin, W. Zhang, W. Zhang, L. Xu, Y. Xue, and W. Li, Mater. Chem. Phys., 277 (2022).

8 P. Zhang, G. Meng, Y. Wang, B. Lei, and F. Wang, Corrosion Communications, 2 72-81 (2021).

9 Y. Deo, S. Guha, K. Sarkar, P. Mohanta, D. Pradhan, and A. Mondal, Appl. Surf. Sci., 515 146078 (2020).

10 N. Rajasekaran and S. Mohan, J. Appl. Electrochem., 39 (10), 1911-1916 (2009).

11 S. Yuan and S. Pehkonen, Corros. Sci., 49 (3), 1276-1304 (2007).

12 K. M. Ismail, A. M. Fathi, and W. A. Badawy, Corros. Sci., 48 (8), 1912-1925 (2006).

13 J.-M. Jang, H.-S. Lee, and J. K. Singh, Materials, 13 (24), 5776 (2020).

14 D. Goranova, G. Avdeev, and R. Rashkov, Surf. Coat. Technol., 240 204-210 (2014).

15 Y. Yang, A. Wang, D. Xiong, Z. Wang, D. Zhou, S. Li, and H.

Zhang, Surf. Coat. Technol., 384 125316 (2020).
16 A. D. Pingale, A. Owhal, A. S. Katarkar, S. U. Belgamwar, and J. S. Rathore, Materials Today: Proceedings, 47 3301-3308 (2021).
17 S. Silaimani, G. Vivekanandan, and P. Veeramani, International Journal of Environmental Science and Technology, 12 2299-2306 (2015).
18 M. Kamel, Z. Anwer, I. Abdel‐Salam, and I. Ibrahim, Surf. Interface Anal., 46 (7), 442-448 (2014).
19 P. Y. Chia, A. Haseeb, and S. H. Mannan, Materials, 9 (6), 430 (2016).
20 S. Ghosh, A. Grover, G. Dey, and M. Totlani, Surf. Coat. Technol., 126 (1), 48-63 (2000).
21 T. Green, A. Russell, and S. Roy, J. Electrochem. Soc., 145 (3), 875 (1998).
22 E. Chassaing, K. V. Quang, and R. Wiart, J. Appl. Electrochem., 17 (6), 1267-1280 (1987).
23 S. Rode, C. Henninot, C. Vallières, and M. Matlosz, J. Electrochem. Soc., 151 (6), C405 (2004).
24 A. Milchev and T. Zapryanova, Electrochim. Acta, 51 (23), 4916-4921 (2006).
25 A. Milchev and T. Zapryanova, Electrochim. Acta, 51 (14), 2926-2933 (2006).
26 V. A. Isaev, O. V. Grishenkova, and Y. P. Zaykov, J. Electroanal. Chem., 818 265-269 (2018).
27 D. Goranova, R. Rashkov, G. Avdeev, and V. Tonchev, Journal of Materials Science, 51 8663-8673 (2016).
28 D. Kong, Z. Zheng, F. Meng, N. Li, and D. Li, J. Electrochem. Soc., 165 (16), D783 (2018).

电流密度和铜离子浓度对电沉积 Cu-Ni 镀层性能的影响

郭叙言[1=]，熊壮壮[1=]，王桂香[1,3,z]，周强[1]，武艳雄[1]，孔德龙[2,z]，马福秋[1]，巫瑞智[3]

(1. 哈尔滨工程大学烟台研究院，山东 烟台 264006)

(2. 枣庄大学，山东 枣庄 277160)

(3. 哈尔滨工程大学超轻材料与表面技术教育部重点实验室，黑龙江 哈尔滨 150001)

摘　要：本文研究了一种简单、高效、环保的防腐技术，通过在工件表面沉积铜镍合金涂层来阻止腐蚀介质，从而保护碳钢表面免受腐蚀。使用扫描电子显微镜、X 射线能量色散光谱、维氏硬度计、摩擦磨损试验机和电化学测试研究了电流密度和 Cu^{2+}浓度对涂层成分、形态和组成的影响。涂层表面出现花椰菜状富镍突起结构。较低的电流密度和 Cu^{2+}浓度通过影响晶粒微观结构和 Cu/Ni 含量来影响涂层的维氏硬度和耐磨性，从而导致硬度和耐磨性能的降低。当电流密度为 10 mA/cm^2，Cu^{2+}浓度为 0.1 mol/L 时，沉积样品的腐蚀电流密度达到 1.389×10^{-5} A·cm^{-2}，经过 24 小时的盐雾试验后，镀层表面腐蚀损伤明显小于未覆盖镀层样品。对沉积机理的研究表明，Cu^{2+}在扩散控制下经历瞬时成核，倾向于垂直生长并形成花椰菜状突起，而 Ni^{2+}则受电化学控制，在表面均匀放电。

关键词：Cu-Ni镀层，腐蚀防护，形态，性能

作者简介：郭叙言，男，1999 年生，硕士，哈尔滨工程大学烟台研究院，山东 烟台 264006，E-mail: gxy321517181@hrbeu.edu.cn